MULTIPLE POTENTIAL WELL STRUCTURE IN INERTIAL ELECTROSTATIC CONFINEMENT DEVICES

A Thesis presented to the Faculty of the Graduate School
University of Missouri-Columbia

In Partial Fulfillment
Of the Requirements for the Degree

Master of Science

---

by

RYAN M. MEYER

Dr. Sudarshan K. Loyalka, Thesis Supervisor
Dr. Mark A. Prelas, Thesis Supervisor

DECEMBER 2004

The undersigned, appointed by the Dean of the Graduate School,
have examined the thesis entitled.

MULTIPLE POTENTIAL WELL STRUCTURE IN INERTIAL

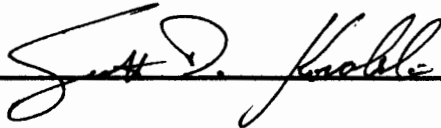## ELECTROSTATIC CONFINEMENT DEVICES

Presented by Ryan Meyer

A candidate for the degree of Master of Science

And hereby certify that in their opinion it is worthy of acceptance.

ACKNOWLEDGEMENTS

TABLE OF CONTENTS

LIST OF ILLUSTRATIONS

LIST OF TABLES

MULTIPLE POTENTIAL WELL STRUCTURE IN INERTIAL ELECTROSTATIC
CONFINEMENT DEVICES

Ryan M. Meyer

Dr. Sudarshan Loyalka, Thesis Supervisor
Dr. Mark Prelas, Thesis Supervisor

ABSTRACT

Inertial Electrostatic Confinement (IEC) devices are of interest as neutron generators for many applications. An essential part of these devices is the formation of a multiple potential well structure within the devices. In this paper, previous analyses of the formation of these wells are reviewed and extended. Three types of IEC systems are classified and analyzed according to the arrangement of electrodes and the species within the system. These systems are the uni-polar cathode-anode (UCA) system, the bi-polar cathode-anode (BCA) system, and the bi-polar anode-cathode (BAC) system. Results of extensive parametric studies are reported through an efficient solution of the Poisson's equation. These results delineate the conditions most conducive for double potential well formation in different systems and may aid in the future design of IEC systems.

I. INTRODUCTION

Inertial Electrostatic Confinement (IEC) devices have many potential applications, including their use as neutron generators. A few of these applications include: luggage inspection, oil well logging, medical isotope production, detection of explosives, archaeometry, forensics, breeding advanced fuels (He3), transmuting long-lived radioactive isotopes from fission reactor waste, a neutron source to drive a sub-critical fission reactor, generating power for space craft, and generating power for terrestrial needs [1]-[9].

Medical isotopes are typically produced on site at a clinic with the use of medical isotope generators, or accelerators. Isotopes used for imaging must be produced on site at the clinic due to the short half-life of typical isotopes employed for medical imaging. The advantages of an IEC device for producing medical isotopes are that it is small, compact, and inexpensive. Such a portable neutron generator can be transported to some of the most remote places on earth in order to treat patients in a relatively inexpensive manner. Another advantage of the IEC is that the radioactivity hazard can effectively be "unplugged", when not in use, thus, special handling, and shielding requirements are limited [10]. Of course, many of these characteristics are desirable features for a number of neutron generator applications. Experiments performed at the University of Wisconsin-Madison have generated 4-8 Bq of N13. Protons of 14.7 MeV, generated by D-He3 reactions, irradiate water flowing through the IEC reactor to produce N13. The isotope, N13, is later separated from the water [7], [8].

In light of these potential applications for the IEC devices, many experimental and theoretical studies have been conducted regarding the potential distribution within IEC reactors. Experiments performed with IEC devices indicate the existence of a multiple potential well structure, within the inner electrode. The general method of theoretically obtaining the potential distribution within a spherical or cylindrical IEC device has been to solve Poisson's equation while simultaneously applying the conditions of current continuity and conservation of energy. These calculations, however, have not consistently supported the formation of double well structures, indicated by experiments [11]-[15]. It is, therefore, of interest to review the previous theoretical work, and to study the well formation in one consistent framework of computations.

Although Langmuir and Blodgett [16] did not study the IEC devices explicitly, their work still provided the basic solutions for potential distribution in the systems of interest. These authors solved Poisson's equation within the inner electrode of a system of concentric spherical electrodes, in a vacuum:

$$\frac{1}{X^2}\frac{d}{dX}X^2\frac{dY}{dX} = \frac{K_e}{X^2}Y^{-1/2};$$ (1)

With the boundary conditions for space charge limited current [17] (i.e. $\frac{\partial V}{\partial r} = 0$ and $V = 0$ at the emitting electrode). In Eq. (1), Y is the normalized potential and X is the normalized radius, given by:

$$Y = \frac{V(r)}{V_a}$$ (2)

$$X = \frac{r}{R_a}$$ (3)

While K_e is defined by Eq. (4), where I_e is the electron current, m_e is the electron mass,

$$K_e = \frac{I_e}{V_a^{3/2}} \left(\frac{m_e}{2e} \right)^{1/2} \frac{1}{4\pi\varepsilon_0} \qquad (4)$$

e is the magnitude of the electron charge, while V_a and R_a are the anode voltage and radius, respectively. The typical solution generated by Langmuir's and Blodgett's equation, Eq. (1), is provided in Fig. 1 for the region within an inner anode.
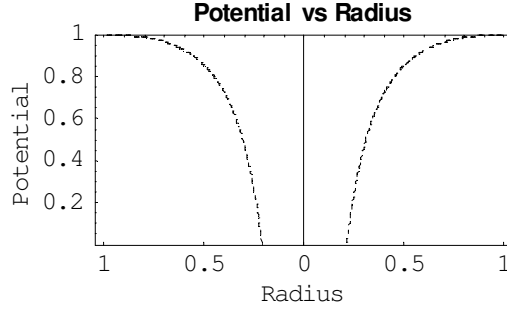
Figure 1: Langmuir's and Blodgett's solution to Poisson's
Equation for concentric spherical electrodes [16].

Hirsch [11] considered a system involving ion injection into a grounded vacuum chamber and electron emission from the inner surface of the chamber wall. For his model, Hirsch constructed the equation, for the region within an inner cathode,

$$\frac{1}{X^2}\frac{d}{dX}X^2\frac{dY}{dX} = \frac{K_i}{X^2}[Y^{-1/2} - \lambda_i(1-Y)^{-1/2}] ; \qquad (5)$$

along with the boundary conditions for space charge limited current [17]:

$$Y(1) = 0, \frac{dY(1)}{dX} = 0 \qquad (6)$$

Here λ_i, and K_i are defined by

$$\lambda_i = \frac{I_e}{I_i} \left(\frac{m_e}{m_i} \right)^{1/2} \qquad (7)$$

$$K_i = \frac{I_i}{V_c^{3/2}} \left(\frac{m_i}{2e} \right)^{1/2} \frac{1}{4\pi\varepsilon_0} \qquad (8)$$

3

and the normalized potential is redefined in Eq (9), as:

$$Y = \frac{-V(r)}{V_c} \tag{9}$$

In Eqs. (7-9), I_i is the ion current, m_i is the ion mass and $-V_c$ is the cathode potential.

Hirsch found that the solution to the boundary value problem, defined by Eqs. (5) and (6), consists of a double potential well structure within the inner cathode, as shown in Fig. 2.
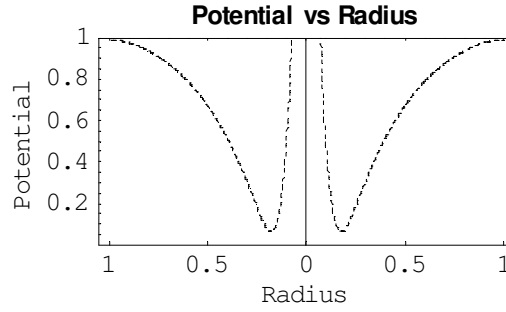
Figure 2: Hirsch's solution to Poisson's Equation for ions injected from a spherical vacuum chamber, with electrons emitted from the inner surface of the vacuum chamber [11].

Hirsch's model neglects spreads in the total and angular energies of the particles. However, Dolan, [15], [18] Lavrent'yev, [19] and Swanson, [13]-[14] created more realistic models that allow for spreads in the total and angular energies of particles. Dolan and Swanson solved Eqs. (10), and (11)

$$\frac{1}{X^2} \frac{d}{dX} X^2 \frac{dY}{dX} = f_e(X,Y) \tag{10}$$

$$\frac{1}{X^2} \frac{d}{dX} X^2 \frac{dY}{dX} = f_e(X,Y) - g_i(X,Y) \tag{11}$$

where $f_e(X,Y)$, and $g_i(X,Y)$ are given as

4

$$f_e(X,Y) = \frac{V_a}{4\pi\varepsilon_o\left(\frac{2eV_a}{m_e}\right)^{1/2}} \cdot$$

$$\int_0^Y dY_{e,E} \int_0^{X^2(Y-Y_{e,E})} dY_{e,\phi} \frac{I_e(Y_{e,E},Y_{e,\phi})}{X^2[Y-Y_{e,E}-(Y_{e,\phi}/X^2)]^{1/2}}$$

(12)
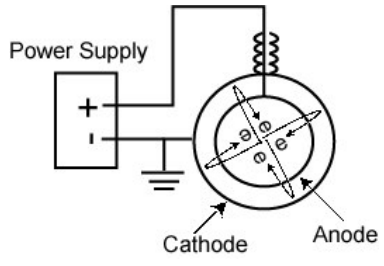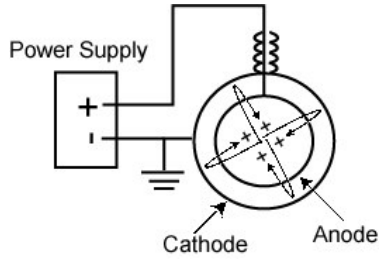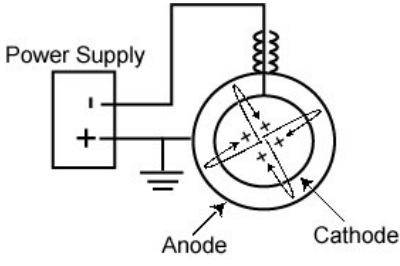
$$g_i(X,Y) = \frac{V_a}{4\pi\varepsilon_o\left(\frac{2eV_a}{m_A}\right)^{1/2}} \cdot$$

$$\int_Y^1 dY_{i,E} \int_0^{X^2(Y_{i,E}-Y)} dY_{i,\phi} \frac{I_i(Y_{i,E},Y_{i,\phi})}{X^2[Y_{i,E}-Y-(Y_{i,\phi}/X^2)]^{1/2}}$$

(13)

for a system with electron emission from an outer grounded cathode and for a system which included ions confined within the inner anode as well as electrons emitted from the outer cathode. The normalized total and angular electron energies are represented by $Y_{e,E}$ and $Y_{e,\phi}$, while the normalized total and angular ion energy is represented by $Y_{i,E}$ and $Y_{i,\phi}$. Equation (10) produces broad single well solutions, while Eq. (11) reveals the formation of double wells under certain conditions.

Swanson's results [13] indicated that double well solutions do form under limited circumstances, however, questions arose pertaining to the uniqueness of the double well solutions. Dynamic IEC analysis by Hockney [20] and Ohnishi [21] indicated that double potential well structures are transient phenomena, thus double well solutions computed in the steady state may not be valid. In addition, simulations by Matsuura [22] revealed that a multiple potential well structure is not necessary to produce multiple radial peaks in the neutron production rate.

In the future, for clarity in system designation, IEC systems will be denoted as shown in Table I:

Table I: This table identifies different types of inertial electrostatic devices that will be analyzed in this work.

Denotation	Electrons	Ions	Schematic
uni-polar cathode-anode system (UCA)	Yes	No	Figure 3: Schematic diagram of a UCA system
bi-polar cathode-anode system (BCA)	Yes	Yes	Figure 4: Schematic diagram of a BCA system
bi-polar anode-cathode system (BAC)	Yes	Yes	Figure 5: Schematic diagram of a BAC system

Thus, the studies performed by Langmuir and Blodgett were for a UCA system, while Hirsch's model is equivalent to the BAC system. In addition, Eq. (10) represents a UCA system and Eq. (11) is for a BCA system.

Our purpose here is to obtain and critically examine potential well solutions within the inner electrodes of the systems in Table I. We also have explored further results for the UCA system and show that we get results similar to those of Dolan and

Swanson [12]-[15]. The method of analysis for the bi-polar systems will involve finding a double well solution and performing systematic variation of certain parameters to determine which parameters affect double well formations the most. We should note that more detailed IEC modeling is performed by simultaneously solving Poisson's equation with equations describing the creation and removal of particles from the system, while the present paper is directed at careful review and analysis of the problem where specific forms of particle distributions are assumed. This work thus serves as a benchmark for more detailed considerations.

II. EQUATIONS AND METHODS OF SOLUTION

For the systems in Table I, the basic problem can be described by Eq. (10) for the UCA system and by Eqs. (11) and (14) for the BCA and BAC systems.

$$\frac{1}{X^2}\frac{d}{dX}X^2\frac{dY}{dX} = f_i(X,Y) - g_e(X,Y) \tag{14}$$

In Eq. (14), $f_i(X,Y)$, and $g_e(X,Y)$ are, respectively;

$$f_i(X,Y) = \frac{V_a}{4\pi\varepsilon_o\left(\frac{2eV_a}{m_e}\right)^{1/2}} \cdot$$

$$\int_0^Y dY_{i,E} \int_0^{X^2(Y-Y_{i,E})} dY_{i,\phi} \frac{I_i(Y_{i,E},Y_{i,\phi})}{X^2[Y-Y_{i,E}-(Y_{i,\phi}/X^2)]^{1/2}} \tag{15}$$

$$g_e(X,Y) = \frac{V_a}{4\pi\varepsilon_o\left(\frac{2eV_a}{m_A}\right)^{1/2}} \cdot$$

$$\int_Y^1 dY_{e,E} \int_0^{X^2(Y_{e,E}-Y)} dY_{e,\phi} \frac{I_e(Y_{e,E},Y_{e,\phi})}{X^2[Y_{e,E}-Y-(Y_{e,\phi}/X^2)]^{1/2}} \tag{16}$$

If we assume guassian distributions for current in Eqs. (12) and (13), then for the systems described by Eqs. (10) and (11), the electron current is distributed over the normalized electron total and angular energies, $Y_{e,E}$ and $Y_{e,\phi}$, as shown in Fig. 6. In addition, the ion current is distributed over $Y_{i,E}$ and $Y_{i,\phi}$, as shown in Fig. 7, where $Y_{i,E}$ and $Y_{i,\phi}$ are the normalized ion total and angular energies, respectively.
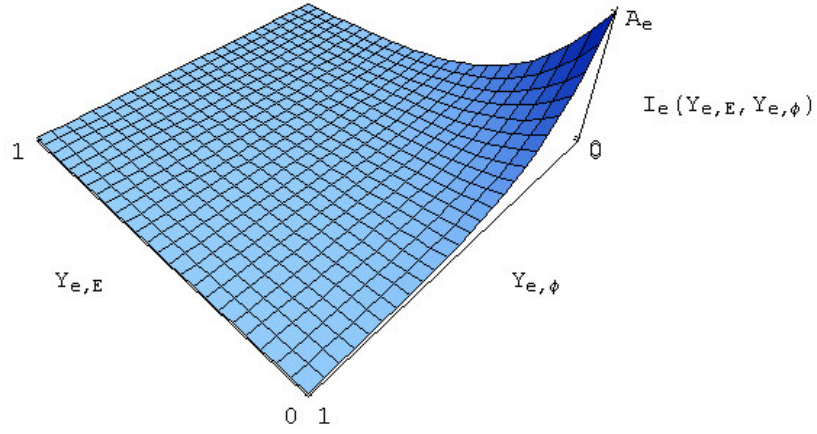
Figure 6: Gaussian electron current distribution over the $Y_{e,E}$, $Y_{e,\phi}$ plane.
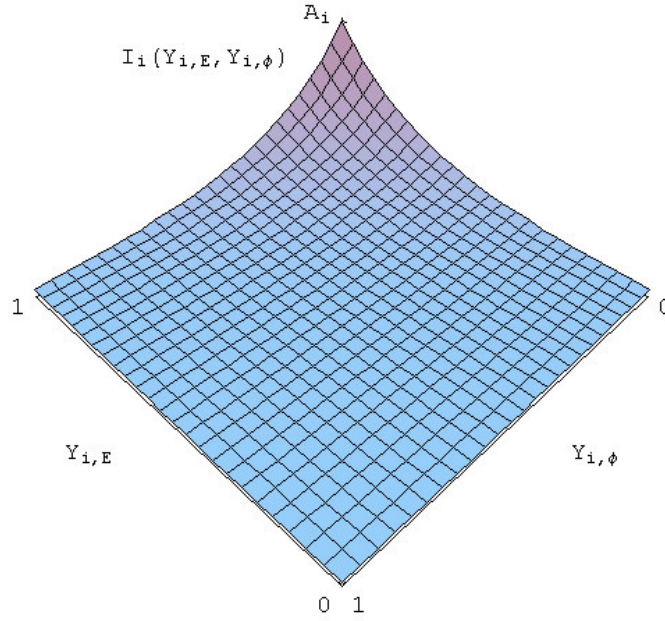
Figure 7: Gaussian ion current distribution over the $Y_{i,E}$, $Y_{i,\phi}$ plane.

The electron current may be represented with Eq. (17),

$$I_e(Y_{e,E}, Y_{e,\phi}) = A_e\, e^{-(Y_{e,E}/\sigma_{e,E})} e^{-(Y_{e,\phi}/\sigma_{e,\phi})} \tag{17}$$

with $\sigma_{e,E}$ and $\sigma_{e,\phi}$ representing the spreads in total and angular electron energy, and where the constant A_e is computed by recognizing that Eq. (18) represents the circulating electron current.

$$I_{ce} = V_a^2 \int\limits_0^1 dY_{e,E} \int\limits_0^{1-Y_{e,E}} dY_{e,\phi} I_e(Y_{e,E}, Y_{e,\phi}) \qquad (18)$$

One thus [13], [14] has for A_e:

$$A_e = \left[I_{ce} / \left(V_a^2\, \sigma_{e,\phi}\, \sigma_{e,E} \right) \right] \cdot$$
$$\left\{ 1 - e^{-(1/\sigma_{e,E})} - \left[\sigma_{e,\phi} / (\sigma_{e,\phi} - \sigma_{e,E}) \right] \cdot \left[e^{-(1/\sigma_{e,\phi})} - e^{-(1/\sigma_{e,E})} \right] \right\}^{-1} \qquad (19)$$

Evaluating A_i is not as straightforward as the evaluation of A_e because the electron is allowed to have $0 \le Y_{e,\phi} \le 1 - Y_{e,E}$ and $0 \le Y_{e,E} \le 1$. The ion has energies in the range $0 \le Y_{i,\phi} \le \left(Y_{i,E} - Y_{\min} \right)$ and $Y_{\min} \le Y_{i,E} \le 1$. These limits depend on the minimum normalized potential within the anode, $Y_{\min}$, which is information that we seek from the solution of Eq. (11). The ion current is represented with Eq. (20), and the circulating ion current is defined in Eq. (21).

$$I_i(Y_{i,E}, Y_{i,\phi}) = A_i\, e^{\left[(Y_{i,E}-1)/\sigma_{i,E} \right]} e^{-(Y_{i,\phi}/\sigma_{i,\phi})} \qquad (20)$$

$$I_{ci} = V_a^2 \int\limits_{Y_{\min}}^1 dY_{i,E} \int\limits_0^{Y_{i,E}-Y_{\min}} dY_{i,\phi} I_i(Y_{i,E}, Y_{i,\phi}) \qquad (21)$$

Observation of Fig. 7 reveals that for small values of energy spreads in the total ion energy and angular ion energy, $\sigma_{i,E}$ and $\sigma_{i,\phi}$, integration of Eq. (21) may be approximated with $Y_{\min} = 0$ for moderate values of $Y_{\min}$ (i.e. $Y_{\min} < 0.85$), which allows us to compute A_i from Eq. (22).

$$A_i = \left[I_{ci} / \left(V_a^2\, \sigma_{i,\phi}\, \sigma_{i,E} \right) \right] \cdot$$
$$\left\{ 1 - e^{-(1/\sigma_{i,E})} + \left[\sigma_{i,\phi} / \left(\sigma_{i,\phi} - \sigma_{i,E} \right) \right] \cdot \left[e^{-(1/\sigma_{i,\phi})} - e^{-(1/\sigma_{i,E})} \right] \right\}^{-1} \qquad (22)$$

If $\sigma_{i,E} = 0.05$ and $\sigma_{i,\phi} = 0.001$, then values of A_i, for values of Y_{min} from 0 to 1 are

provided in Table II.

Table II: A_i versus Y_{min} for $\sigma_{i,E} = 0.05$
and $\sigma_{i,\phi} = 0.001$.

Y_{min}	$A_i/(I_i\, V_a^{-2})$
0	20000
0.1	20000
0.2	20000
0.3	20000
0.4	20000.1
0.5	20000.9
0.6	20006.8
0.7	20050.7
0.8	20380.9
0.85	21070.4
0.9	23204.5
0.95	32019.8

The error in using the approximation $Y_{min} = 0$ when $Y_{min} = 0.85$ is 5.1% and the error in

using $Y_{min} = 0$ when $Y_{min} \leq 0.80$ is $< 1.9\%$. Using Eqs. (17) - (22), we can introduce Eqs.

(23) and (24),

$$f_e(X,Y) =$$

$$\frac{K_e}{X^2}\int_0^Y dY_{e,E} \int_0^{X^2(Y-Y_{e,E})} dY_{e,\phi} \frac{e^{-(Y_{e,E}/\sigma_{e,E})}e^{-(Y_{e,\phi}/\sigma_{e,\phi})}}{[Y-Y_{e,E}-(Y_{e,\phi}/X^2)]^{1/2}} \qquad (23)$$

$$g_i(X,Y) =$$

$$\frac{K_i}{X^2}\int_Y^1 dY_{i,E} \int_0^{X^2(Y_{i,E}-Y)} dY_{i,\phi} \frac{e^{-(Y_{i,E}/\sigma_{i,E})}e^{-(Y_{i,\phi}/\sigma_{i,\phi})}}{[Y_{i,E}-Y-(Y_{i,\phi}/X^2)]^{1/2}} \qquad (24)$$

with K_e and K_i defined in Eqs. (25) and (26), where η represents the transparency of the

anode [15], [18].

$$K_e = [2\eta/(1-\eta^2)] \cdot \{[1/(4\pi\varepsilon_o \sigma_{e,E} \sigma_{e,\phi})] \cdot [m_e/(2e)]^{1/2}\} \cdot$$
$$\{1 - e^{-(1/\sigma_{e,E})} - [\sigma_{e,\phi}/(\sigma_{e,\phi} - \sigma_{e,E})] \cdot [e^{-(1/\sigma_{e,\phi})} - e^{-(1/\sigma_{e,E})}]\}^{-1} \cdot \tag{25}$$
$$(I_e/V_a^{3/2})$$

$$K_i = [2\eta/(1-\eta^2)] \cdot \{[1/(4\pi\varepsilon_o \sigma_{i,E} \sigma_{i,\phi})] \cdot [m_i/(2e)]^{1/2}\} \cdot$$
$$\{1 - e^{-(1/\sigma_{i,E})} + [\sigma_{i,\phi}/(\sigma_{i,\phi} - \sigma_{i,E})] \cdot [e^{-(1/\sigma_{i,\phi})} - e^{-(1/\sigma_{i,E})}]\}^{-1} \cdot \tag{26}$$
$$(I_i/V_a^{3/2})$$

Eqs. (23) and (24) may then be plugged back into Eqs. (10) and (11), respectively, to solve for the potential distribution within the anode of a UCA system and a BCA system.

In the BAC system, represented by Eq. (14), ions and electrons reverse the roles they had in the BCA system of Eq. (11). The distribution of ion current for Eq. (14) is now represented with Fig. 6, and the distribution of electron current is now illustrated in Fig. 7. The ion current is represented with Eq. (27),

$$I_i(Y_{i,E}, Y_{i,\phi}) = A_i\, e^{-(Y_{i,E}/\sigma_{i,E})} e^{-(Y_{i,\phi}/\sigma_{i,\phi})} \tag{27}$$

and the circulating ion current is now defined with Eq. (28).

$$I_{ci} = V_c^2 \int_0^1 dY_{i,E} \int_0^{1-Y_{i,E}} dY_{i,\phi} I_i(Y_{i,E}, Y_{i,\phi}) \tag{28}$$

A_i is surmised from Eq. (28) and defined in Eq. (29).

$$A_i = [I_{ci}/(V_c^2 \sigma_{i,\phi} \sigma_{i,E})] \cdot$$
$$\{1 - e^{-(1/\sigma_{i,E})} - [\sigma_{i,\phi}/(\sigma_{i,\phi} - \sigma_{i,E})] \cdot [e^{-(1/\sigma_{i,\phi})} - e^{-(1/\sigma_{i,E})}]\}^{-1} \tag{29}$$

Electron current is represented in Eq. (30), and the circulating electron current is now defined by Eq. (31).

$$I_e(Y_{e,E}, Y_{e,\phi}) = A_e\, e^{[(Y_{e,E}-1)/\sigma_{e,E}]} e^{-(Y_{e,\phi}/\sigma_{e,\phi})} \tag{30}$$

$$I_{ce} = V_c^2 \int_{Y_{min}}^{1} dY_{e,E} \int_{0}^{Y_{e,E} - Y_{min}} dY_{e,\phi} I_e(Y_{e,E}, Y_{e,\phi}) \tag{31}$$

Analogous to A_i, for the BCA system, a difficulty occurs in determining the value of

A_e, for the BAC system, because ranges for the electron total and angular energies are

$0 \le Y_{e,\phi} \le (Y_{e,E} - Y_{min})$ and $Y_{min} \le Y_{e,E} \le 1$. As in the case of the BCA system, this BAC

system requires knowledge of the minimum normalized potential, which is information

that we seek from the solution of Eq. (14). Thus, Y_{min} is once again approximated with

$Y_{min} = 0$ to obtain the value of A_e in Eq. (32).:

$$
\begin{aligned}
A_e = &\left[I_{ce} / \left(V_c^2 \, \sigma_{e,\phi} \, \sigma_{e,E} \right) \right] \cdot \\
&\left\{ 1 - e^{-(1/\sigma_{e,E})} + \left[\sigma_{e,\phi} / \left(\sigma_{e,\phi} - \sigma_{e,E} \right) \right] \cdot \left[e^{-(1/\sigma_{e,\phi})} - e^{-(1/\sigma_{e,E})} \right] \right\}^{-1}
\end{aligned}
\tag{32}
$$

This assumption leads to errors in the calculations of A_e of ~40% for large values of

Y_{min} (~0.85). An error of 40% will produce a noticeable difference in the solution, but, it

will not produce a change in the trends observed. In addition, since the error decreases

exponentially as the value of Y_{min} decreases, error in the calculation of A_e for the BAC

system, does not produce a noticeable change in the solution for small values of Y_{min}. A

table with values of A_e calculated using various values of Y_{min} is given in Table III.

Table III: A_e versus Y_{min} for $\sigma_{e,E} = 0.15$ and $\sigma_{e,\phi} = 0.001$.

Y_{min}	$A_e/(I_e V_c^{-2})$
0	6675.22
0.1	6683.34
0.2	6699.23
0.3	6730.38
0.4	6791.9
0.5	6915.01
0.6	7168.07
0.7	7718.23
0.8	9074.82
0.85	10587.9
0.9	13798.7
0.95	23924.0

In parallel with Eqs. (23) and (24), for BCA systems, we obtain Eqs. (33) and (34) to be plugged into Eq. (14).

$$f_i(X,Y) =$$

$$\frac{K_i}{X^2} \int_0^Y dY_{i,E} \int_0^{X^2(Y-Y_{i,E})} dY_{i,\phi} \frac{e^{-(Y_{i,E}/\sigma_{i,E})} e^{-(Y_{i,\phi}/\sigma_{i,\phi})}}{[Y - Y_{i,E} - (Y_{i,\phi}/X^2)]^{1/2}} \tag{33}$$

$$g_e(X,Y) =$$

$$\frac{K_e}{X^2} \int_Y^1 dY_{e,E} \int_0^{X^2(Y_{e,E}-Y)} dY_{e,\phi} \frac{e^{-(Y_{e,E}/\sigma_{e,E})} e^{-(Y_{e,\phi}/\sigma_{e,\phi})}}{[Y_{e,E} - Y - (Y_{e,\phi}/X^2)]^{1/2}} \tag{34}$$

The values of K_i and K_e for Eqs. (33) and (34), respectively, are defined in Eqs. (35) and (36), where η is the transparency of the cathode.

$$K_i = [2\eta/(1-\eta^2)] \cdot \left\{ [1/(4\pi\varepsilon_o \sigma_{i,E} \sigma_{i,\phi})] \cdot [m_i/(2e)]^{1/2} \right\} \cdot$$
$$\left\{ 1 - e^{-(1/\sigma_{i,E})} - [\sigma_{i,\phi}/(\sigma_{i,\phi} - \sigma_{i,E})] \cdot [e^{-(1/\sigma_{i,\phi})} - e^{-(1/\sigma_{i,E})}] \right\}^{-1} \cdot \tag{35}$$
$$(I_i/V_c^{3/2})$$

$$K_e = \left[2\eta/\left(1-\eta^2\right)\right] \cdot \left\{\left[1/\left(4\pi\varepsilon_o\,\sigma_{e,E}\,\sigma_{e,\phi}\right)\right] \cdot \left[m_e/(2e)\right]^{1/2}\right\} \cdot$$
$$\left\{1-e^{-\left(1/\sigma_{e,E}\right)} + \left[\sigma_{e,\phi}/\left(\sigma_{e,\phi}-\sigma_{e,E}\right)\right] \cdot \left[e^{-\left(1/\sigma_{e,\phi}\right)} - e^{-\left(1/\sigma_{e,E}\right)}\right]\right\}^{-1} \cdot \qquad (36)$$
$$\left(I_e/V_c^{3/2}\right)$$

Equations (10), (11), and (14) are solved numerically. The double integrals on the right hand sides of Eqs. (23), (24), (33) and (34) have been previously evaluated by expanding the exponential into a Taylor Series. After Taylor series expansion, the integral of the resulting argument may be found using a standard table of integrals [13]. However, we have found that it is possible to express the double integrals on the right hand sides of Eqs. (23), (24), (33), (34) in terms of error functions for which fast and accurate numerical routines are readily available. Thus, for $g_i(X,Y)$ and $g_e(X,Y)$, we have:

$$g_i(X,Y) = \left(K_i/X\right) \cdot \left[\left(\pi^{1/2}\,\sigma_{i,E}\,\sigma_{i,\phi}\right)/\left(\sigma_{i,\phi}-\sigma_{i,E}\,X^2\right)\right] \cdot$$
$$\left\{\begin{array}{c} \sigma_{i,\phi}^{1/2} \cdot e^{\left[X^2(Y-1)/\sigma_{i,\phi}\right]} \cdot Erfi[X(1-Y)^{1/2}/\sigma_{i,\phi}^{1/2}] - \\ \sigma_{i,E}^{1/2}\,e^{\left[(Y-1)/\sigma_{i,E}\right]} \cdot X \cdot Erfi[(1-Y)^{1/2}/\sigma_{i,E}^{1/2}] \end{array}\right\} \qquad (37)$$

$$g_e(X,Y) = \left(K_e/X\right) \cdot \left[\left(\pi^{1/2}\,\sigma_{e,E}\,\sigma_{e,\phi}\right)/\left(\sigma_{e,\phi}-\sigma_{e,E}\,X^2\right)\right] \cdot$$
$$\left\{\begin{array}{c} \sigma_{e,\phi}^{1/2} \cdot e^{\left[X^2(Y-1)/\sigma_{e,\phi}\right]} \cdot Erfi[X(1-Y)^{1/2}/\sigma_{e,\phi}^{1/2}] - \\ \sigma_{e,E}^{1/2}\,e^{\left[(Y-1)/\sigma_{e,E}\right]} \cdot X \cdot Erfi[(1-Y)^{1/2}/\sigma_{e,E}^{1/2}] \end{array}\right\} \qquad (38)$$

where $Erfi[z]$ is the imaginary error function, which is defined in Eq. (39), where $Erf[z]$ is the error function.

$$Erfi[z] = \frac{Erf[i\,z]}{i} \qquad (39)$$

Similarly for $f_e(X,Y)$ and $f_i(X,Y)$ we find:

$$f_e(X,Y) = (K_e/X) \cdot \left[\left(\pi^{1/2}\, \sigma_{e,E}\, \sigma_{e,\phi} \right) / \left(\sigma_{e,\phi} - \sigma_{e,E}\, X^2 \right) \right] \cdot$$
$$\left\{ \begin{array}{l} \sigma_{e,\phi}^{1/2} \cdot e^{-\left(X^2 Y / \sigma_{e,\phi} \right)} \cdot Erfi[X\,Y^{1/2} / \sigma_{e,\phi}^{1/2}] - \\ \quad \sigma_{e,E}^{1/2}\, e^{-\left(Y / \sigma_{e,E} \right)} \cdot X \cdot Erfi[Y^{1/2} / \sigma_{e,E}^{1/2}] \end{array} \right\} \tag{40}$$

$$f_i(X,Y) = (K_i/X) \cdot \left[\left(\pi^{1/2}\, \sigma_{i,E}\, \sigma_{i,\phi} \right) / \left(\sigma_{i,\phi} - \sigma_{i,E}\, X^2 \right) \right] \cdot$$
$$\left\{ \begin{array}{l} \sigma_{i,\phi}^{1/2} \cdot e^{-\left(X^2 Y / \sigma_{i,\phi} \right)} \cdot Erfi[X\,Y^{1/2} / \sigma_{i,\phi}^{1/2}] - \\ \quad \sigma_{i,E}^{1/2}\, e^{-\left(Y / \sigma_{i,E} \right)} \cdot X \cdot Erfi[Y^{1/2} / \sigma_{i,E}^{1/2}] \end{array} \right\} \tag{41}$$

These results dramatically reduce computational labor and increase computational speed. In addition, they increase the accuracy and reliability of solutions obtained.

Equations (37), (38), (40), and (41) can be inserted into Eqs. (10), (11) and (14). The latter equations are then solved numerically by assuming the boundary condition in Eq. (42),

$$\frac{dY(0)}{dX} = 0 \tag{42}$$

and employing the shooting method to determine the value of $Y(0)$ that satisfies the boundary condition of Eq. (43).

$$Y(1) = 1 \tag{43}$$

The models just described, for each of the systems in Table I, are summarized in Table IV.

Table IV: A summary of the systems and corresponding equations.

System	Model	Right Hand Side of Model
UCA	$\dfrac{1}{X^2}\dfrac{d}{dX}X^2\dfrac{dY}{dX} = f_e(X,Y)$	Use $f_e(X,Y)$ in Eq. (40), with K_e in Eq. (25).
BCA	$\dfrac{1}{X^2}\dfrac{d}{dX}X^2\dfrac{dY}{dX} = f_e(X,Y) - g_i(X,Y)$	• Use $f_e(X,Y)$ in Eq. (40), with K_e in Eq. (25). • Use $g_i(X,Y)$ in Eq. (37) with K_i in Eq. (26).
BAC	$\dfrac{1}{X^2}\dfrac{d}{dX}X^2\dfrac{dY}{dX} = f_i(X,Y) - g_e(X,Y)$	• Use $f_i(X,Y)$ in Eq. (41), with K_i in Eq. (35). • Use $g_e(X,Y)$ in Eq. (38) with K_e in Eq. (36).

In order to study double well solutions for Eqs. (11) and (14), it is convenient to introduce some measures. A central well will provide better confinement if the peak of the well is large and the well is narrow in width. The width of a central double well is depicted in Figure 8,
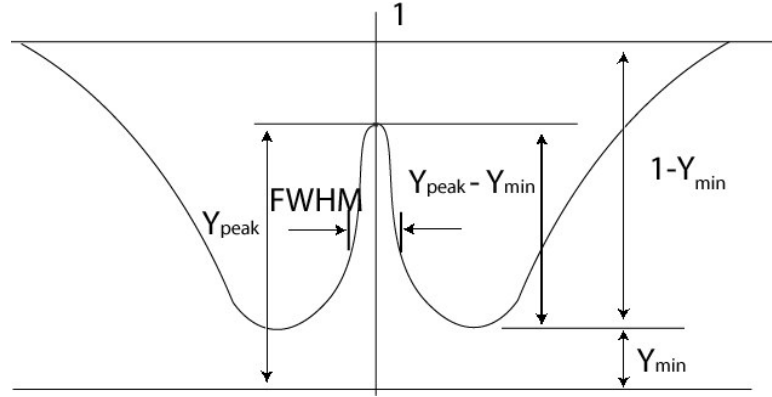

Figure 8: Depiction of a typical double well solution.

and is defined as the Full Width at Half Maximum (FWHM). The value of half-maximum is the average of the central well peak potential and the minimum potential within the well. The "Double Well Depth" (DWD) is defined by Tzonev [22] in Eq. (44), and is depicted in Figure 8.

$$DWD = \frac{Y_{peak} - Y_{min}}{1 - Y_{min}} \qquad (44)$$

III. RESULTS

Solutions for systems considered in Table IV will be provided in this section. A parameter for each system will be varied, while the rest of the parameters are held constant. Thus, several plots are generated for each of the models in Table IV, revealing trends in IEC behavior. The FWHM and DWD of solutions in a particular plot are provided in a corresponding table. We begin by discussing the results for the UCA system, and then provide the results for the BCA and BAC models.

A. UCA System:

The solutions to Eq. (10) for different values of $\sigma_{e,E}$, $\sigma_{e,\phi}$, I_e, and V_a are shown in Figs. 9-12. Figure 9 shows several solutions to the UCA model for values of $\sigma_{e,\phi}$ over the range of $0.0005 \le \sigma_{e,\phi} \le 0.8$. Solutions, for multiple values of $\sigma_{e,E}$, where $0.01 \le \sigma_{e,E} \le 0.8$ are shown in Fig. 10. Figure 11 contains solutions for UCA model as the voltage is varied from $50 \le V_a \le 2000$ V, while Fig. 12 contains solutions for several values of current, with $25 \le I_e \le 375$ mA.

Figure 9 shows that the solution is highly dependent on the angular energy spread, and, as the angular energy spread of electrons decreases, the solution of Eq. (10) approaches the solution of Langmuir and Blodgett [16] in Fig. 1. Variation in the total energy spread of electrons has very little effect on the potential well shape as indicated in Fig. 10. Figures 11 and 12 show that potential well depth varies proportionally to the perveance, $\dfrac{I_e}{V_a^{3/2}}$.

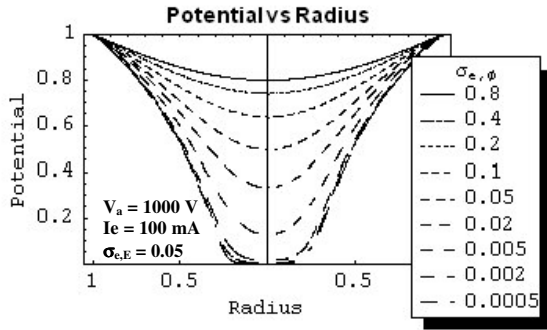Figure 9: Potential vs. Radius within the anode of the UCA model as a function of angular energy spread.
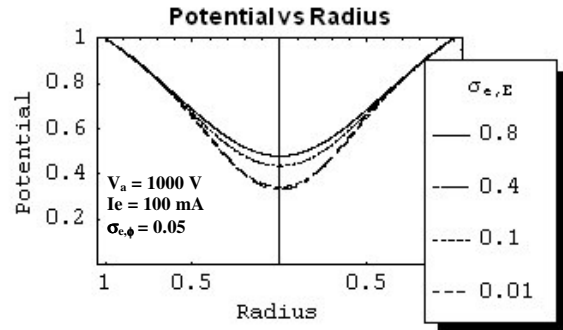

Figure 10: Potential vs. Radius within the anode of the UCA model as a function of total energy spread.
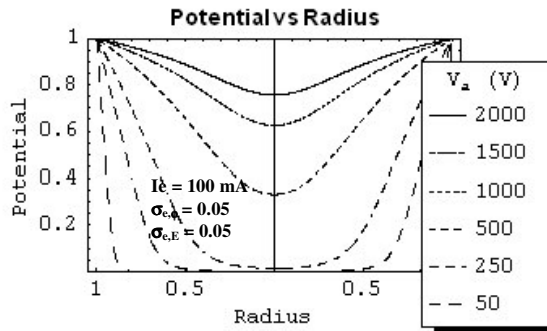

Figure 11: Potential vs. Radius within the anode of the UCA model as a function of applied voltage.
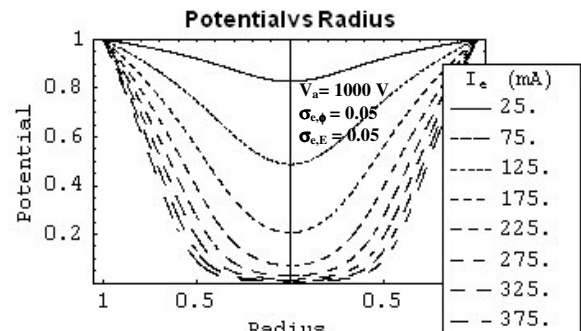
Figure 12: Potential vs. Radius within the anode of the UCA model as a function of current.

B.   BCA System:

Each one of the parameters, $\sigma_{e,\phi}$, $\sigma_{e,E}$, $\sigma_{i,\phi}$, $\sigma_{i,E}$, I_e, V_a, and β (ratio of the ion

current to electron current, $\dfrac{I_i}{I_e}$), are varied, while the rest are held constant to observe

trends in the solution of Eq. (11). Figure 13 shows solutions for the BCA system for

various values of $\sigma_{i,\phi}$ in the range $0.001 \leq \sigma_{i,\phi} \leq 0.5$, and Table V provides a list of their

FWHM's and DWD's. Fig.14 contains several solutions for $\sigma_{i,E}$ over $0.01 \leq \sigma_{i,E} \leq 0.8$,

with the FWHM and DWD of each solution listed in Table VI. Electron angular energy

is varied from $0.01 \leq \sigma_{e,\phi} \leq 0.5$ and solutions for these values are given in Fig. 15, with the

associated FWHM and DWD data provided in Table VII. Next, solutions for $\sigma_{e,E}$ over

$0.05 \leq \sigma_{e,E} \leq 0.8$ are shown in Fig. 16, and the FWHM's and DWD's for these solutions

are given in Table VIII. The ratio of ion current to electron current, β, is varied for

$0 \leq \beta \leq 0.003$ and solutions are given in Fig. 17, while the FWHM and DWD data for

these solutions are given in Table IX. The applied voltage is varied for $400 \leq V_a \leq 1500$

volts and solutions are given in Fig. 18, with a list of the FWHM's and DWD's given in

Table X.   Finally, Eq. (11) is solved for several values of electron current,

$100 \leq I_e \leq 400 \, \text{mA}$, and the solutions are displayed in Fig. 19, with a list of the FWHM's

and DWD's provided in Table XI.

Potential vs Radius

Figure 13: Potential vs. Radius within the anode of the BCA model as a function of ion angular energy spreads.

Potential vs Radius

Figure 14: Potential vs. Radius within the anode of the BCA model as a function of ion total energy spreads.

Potential vs Radius

Figure 15: Potential vs. Radius within the anode of the BCA model as a function of electron angular energy spreads.

Potential vs Radius

Figure 16: Potential vs. Radius within the anode of the BCA model as a function of electron total energy spreads.

Potential vs Radius
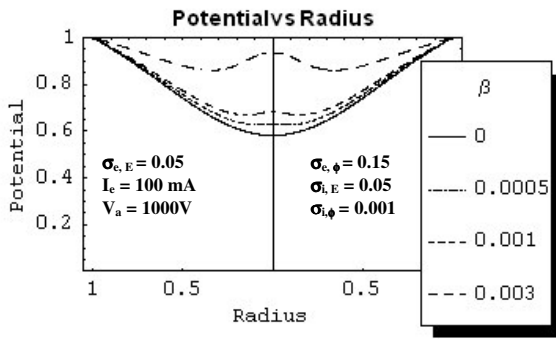
Figure 17: Potential vs. Radius within the anode of the BCA model as a function of β.

Potential vs Radius

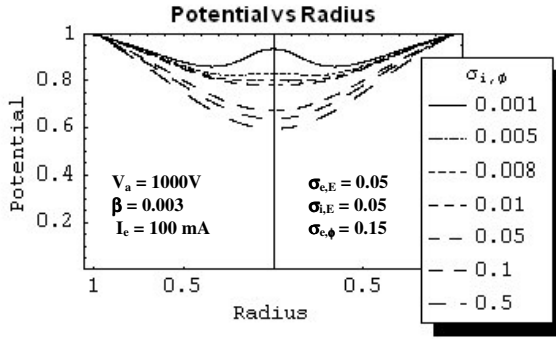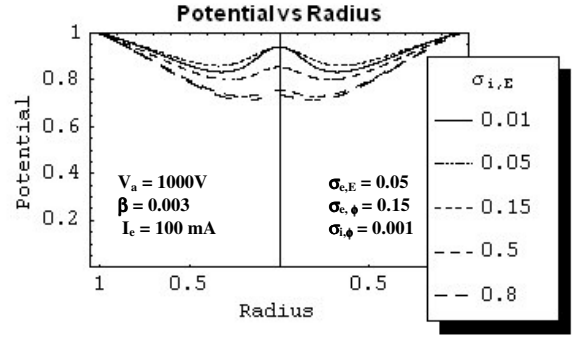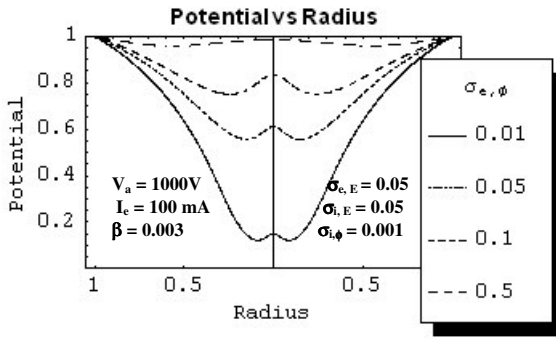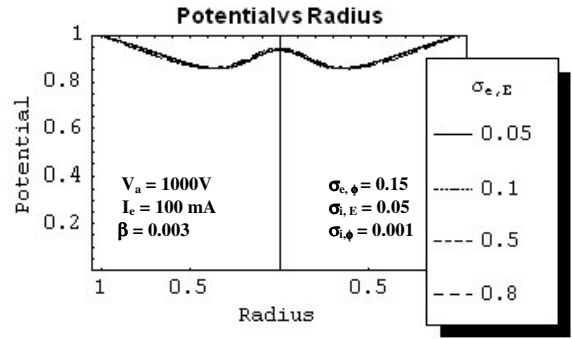Figure 18: Potential vs. Radius within the anode of the BCA model as a function of voltage.

Potential vs Radius

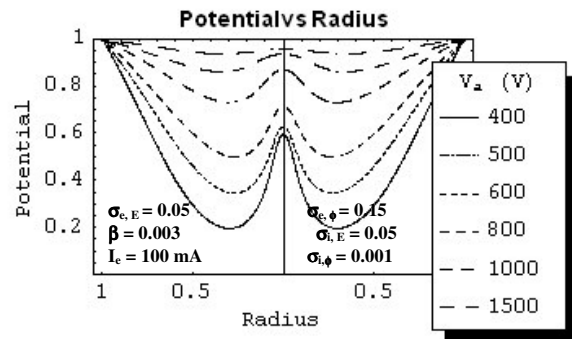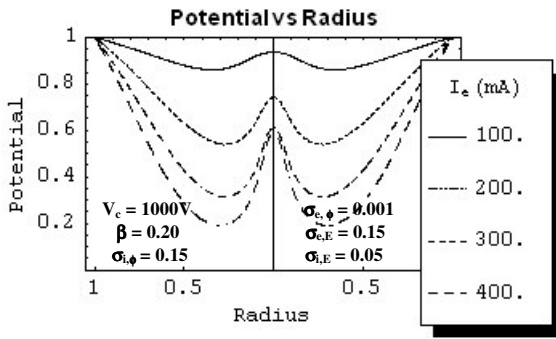Figure 19: Potential vs. Radius within the anode of the BCA model as a function of electron current.

21

Table V: DWD and FWHM for the BCA model, for several values of ion angular energy spread, as shown in Fig. 13.

$\sigma_{i,\phi}$	Y_{min}	Y_{peak}	DWD	FWHM
0.001	0.860	0.935	0.538	0.313
0.005	0.824	0.833	0.053	0.239
0.008	0.799	0.799	-	-
0.010	0.783	0.783	-	-
0.050	0.672	0.672	-	-
0.100	0.637	0.637	-	-
0.500	0.594	0.594	-	-

Table VI: DWD and FWHM for the BCA model, for several values of ion total energy spread, as shown in Fig. 14.

$\sigma_{i,E}$	Y_{min}	Y_{peak}	DWD	FWHM
0.010	0.833	0.940	0.641	0.271
0.050	0.860	0.935	0.538	0.313
0.150	0.800	0.855	0.272	0.242
0.500	0.729	0.756	0.099	0.184
0.800	0.713	0.733	0.072	0.170

Table VII: DWD and FWHM for the BCA model, for several values of electron angular energy spread, as shown in Fig. 15.

$\sigma_{e,\phi}$	Y_{min}	Y_{peak}	DWD	FWHM
0.010	0.122	0.150	0.032	0.077
0.050	0.557	0.610	0.121	0.127
0.100	0.751	0.832	0.326	0.204
0.500	0.959	0.984	0.617	0.610

Table VIII: DWD and FWHM for the BCA model, for several values of electron total energy spread, as shown in Fig. 16.

$\sigma_{e,E}$	Y_{min}	Y_{peak}	DWD	FWHM
0.050	0.860	0.935	0.538	0.313
0.100	0.857	0.935	0.545	0.314
0.500	0.858	0.942	0.591	0.341
0.800	0.862	0.945	0.603	0.352

Table IX: DWD and FWHM for the BCA model for several values of β, as shown in Fig. 17.

β	Y_{min}	Y_{peak}	DWD	FWHM
0	0.582	0.582	-	-
0.0005	0.632	0.632	-	-
0.001	0.669	0.685	0.050	0.132
0.003	0.860	0.935	0.538	0.313

Table X: DWD and FWHM for the BCA model for several values of applied voltage, as shown in Fig. 18.

V_a (volts)	Y_{min}	Y_{peak}	DWD	FWHM
400	0.196	0.595	0.496	0.173
500	0.345	0.626	0.429	0.173
600	0.498	0.715	0.431	0.185
800	0.730	0.870	0.518	0.240
1000	0.860	0.935	0.538	0.313
1500	0.936	0.956	0.310	0.335

Table XI: DWD and FWHM for the BCA model for several values electron current, as shown in Fig. 19.

I_e (mA)	Y_{min}	Y_{peak}	DWD	FWHM
100	0.860	0.935	0.538	0.313
200	0.540	0.742	0.439	0.191
300	0.315	0.613	0.435	0.172
400	0.191	0.596	0.500	0.173

Figures 13-19 and Tables V-XI show that a double well solution depends most greatly on the value of $\sigma_{i,\phi}$. A double well structure exists for small values of $\sigma_{i,\phi}$, and vanishes rapidly as $\sigma_{i,\phi}$ is increased. Small values of $\sigma_{e,\phi}$ tend to deepen the minimum depth of the potential well, but small values of $\sigma_{e,\phi}$ do not necessarily enhance the distinctness of the central double well. Results in Table VII shows that that for $\sigma_{e,\phi}$=0.01, the FWHM of the solution is smallest for solutions in Figure 15, but its DWD is rather poor. On the other hand, the solution for $\sigma_{e,\phi}$= 0.5 has the best DWD value for solutions of Figure 15, but it has a very wide FWHM. As a general observation, it appears to be undesirable to have $\sigma_{e,\phi}$ too small, possibly because the existence of more electrons in the center of the device may neutralize the positive ions trapped in the double well.

The value of $\sigma_{i,E}$ has a noticeable effect on the central double well, but the double well solution does not vanish nearly as rapidly for increasing values of $\sigma_{i,E}$ as it does for increasing values of $\sigma_{i,\phi}$. In fact, double well solutions still exist for relatively large values of $\sigma_{i,E}$. The existence of a double well appears to be nearly independent of $\sigma_{e,E}$ according to the solutions in Fig. 16, while Figs. 18 and 19 reveal that the distinctness of the double well solution is proportional to the system perveance, $\dfrac{I_e}{V_a^{3/2}}$.

C.   BAC System:

Each one of the parameters, $\sigma_{e,\phi}$, $\sigma_{e,E}$, $\sigma_{i,\phi}$, $\sigma_{i,E}$, I_i, V_c, and β, is varied, with the rest held constant to observe trends in the solution of Eq. (14) for the BAC system.

Figure 20 shows solutions for the BAC system for various values of $\sigma_{e,\phi}$ in the range $0.0005 \leq \sigma_{e,\phi} \leq 0.1$ and Figure 21 contains several solutions for $\sigma_{e,E}$ over $0.01 \leq \sigma_{e,E} \leq 0.5$. Ion angular energy is varied from $0.06 \leq \sigma_{i,\phi} \leq 0.2$ and solutions for these values are given in Fig. 22. Next, solutions for $\sigma_{i,E}$ over $0.01 \leq \sigma_{i,E} \leq 0.3$ are shown in Fig. 23. β is varied for $0.125 \leq \beta \leq 1.25$ and solutions are given in Fig. 24, and the applied voltage is varied for $500 \leq V_c \leq 1200$ V with solutions given in Fig. 25. Finally, Eq. (14) is solved for many values of ion current, $2 \leq I_i \leq 7.2$ mA, and the solutions are displayed in Fig. 26. FWHM and DWD data for the solutions in Figs. 20-26 are provided in Tables XII through XVIII.

In Fig. 20, it is evident that the existence of a double well structure depends rather strongly on, $\sigma_{e,\phi}$, since the central peak in Fig. 20 vanishes rapidly as the angular energy of the electrons increases. Well depth increases substantially for decreasing values of $\sigma_{i,\phi}$, in Fig. 22, but the DWD of the solution is also degraded. A double well solution is unable to materialize for $\sigma_{e,E} = 0.01$ and $\sigma_{e,E} = 0.05$. However, Fig. 21 shows that a double well solution appears at approximately $\sigma_{e,E} = 0.1$, and the quality of the well then degrades for increasing values of $\sigma_{e,E}$. Fig. 23 reveals that the value of $\sigma_{i,E}$ has minimal effects on the potential well structure, while Figs. 25 and 26 reveal that the distinctness of a double well varies with proportion to the perveance, $\dfrac{I_i}{V_c^{3/2}}$.
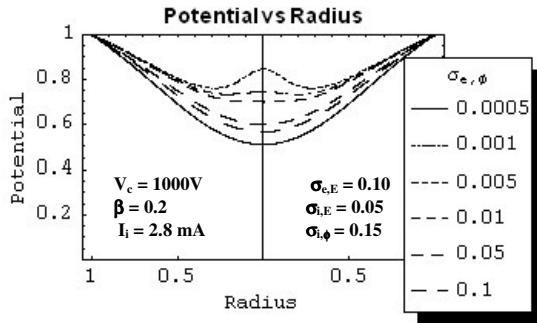
Figure 20: Potential vs. Radius within the cathode of the BAC model as a function of spread in angular electron energy.

Figure 21: Potential vs. Radius within the cathode of the BAC model as a function of spread in total electron energy.

Figure 22: Potential vs. Radius within the cathode of the BAC model as a function of spread in angular ion energy.

Figure 23: Potential vs. Radius within the cathode of the BAC model as a function of spread in total ion energy.

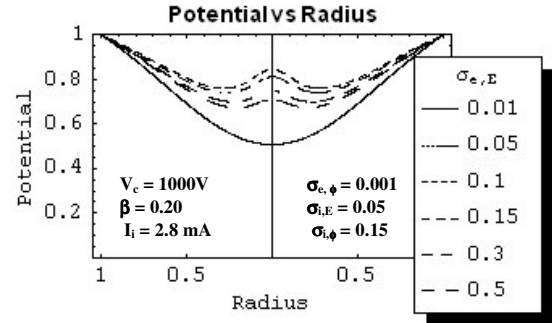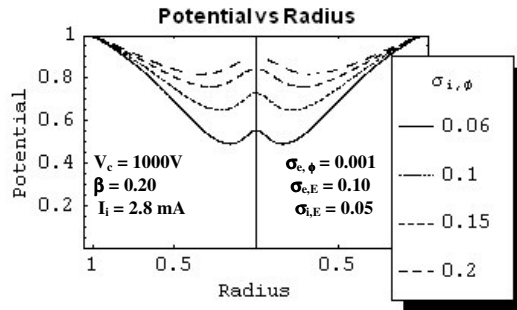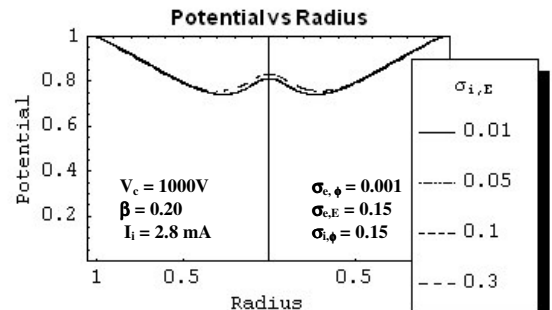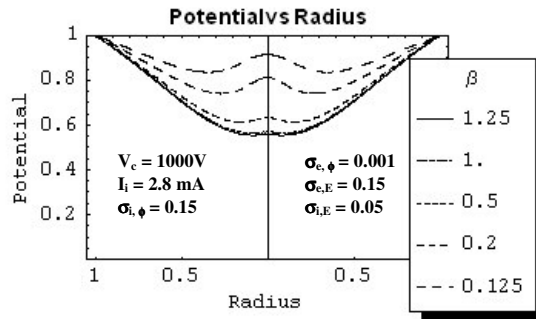**Figure 24:** Potential vs. Radius within the cathode of the BAC model as a function of β.
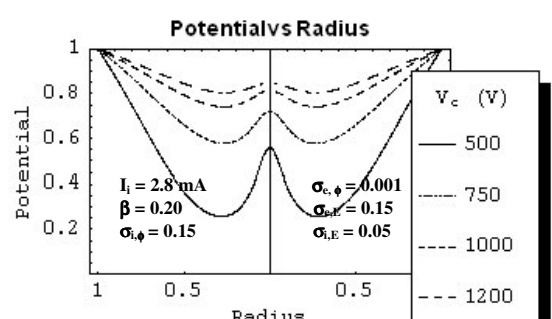
Figure 25: Potential vs. Radius within the cathode of the BAC model as a function of applied voltage.
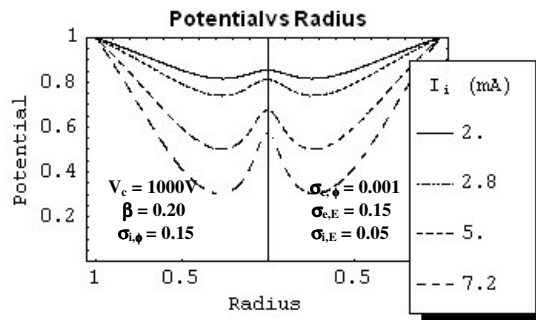
Figure 26: Potential vs. Radius within the cathode of the BAC system as a function of ion current.

25

Table XII: DWD and FWHM for the BAC model for several values of electron angular energy spread, as shown in Fig. 20.

$\sigma_{e,\phi}$	Y_{min}	Y_{peak}	DWD	FWHM
0.0005	0.508	0.508	-	-
0.001	0.760	0.845	0.353	0.238
0.005	0.732	0.743	0.042	0.213
0.010	0.699	0.699	-	-
0.050	0.598	0.598	-	-
0.100	0.564	0.564	-	-

Table XIII: DWD and FWHM for the BAC model for several values of electron total energy spread, as shown in Fig. 21.

$\sigma_{e,E}$	Y_{min}	Y_{peak}	DWD	FWHM
0.01	0.508	0.508	-	-
0.05	0.508	0.508	-	-
0.10	0.760	0.845	0.353	0.238
0.15	0.741	0.812	0.275	0.224
0.30	0.700	0.749	0.163	0.197
0.50	0.674	0.710	0.112	0.181

Table XIV: DWD and FWHM for the BAC model for several values of ion angular energy spread, as shown in Fig. 22.

$\sigma_{i,\phi}$	Y_{min}	Y_{peak}	DWD	FWHM
0.06	0.491	0.555	0.125	0.132
0.10	0.650	0.730	0.229	0.179
0.15	0.760	0.845	0.353	0.238
0.20	0.820	0.898	0.434	0.290

Table XV: DWD and FWHM for the BAC model for several values of ion total energy spread, as shown in Fig. 23.

$\sigma_{i,E}$	Y_{min}	Y_{peak}	DWD	FWHM
0.01	0.741	0.811	0.271	0.222
0.05	0.741	0.812	0.275	0.224
0.10	0.741	0.814	0.282	0.228
0.30	0.757	0.832	0.310	0.245

Table XVI: DWD and FWHM for the BAC model for several values of β, as shown in Fig. 24.

β	Y_{min}	Y_{peak}	DWD	FWHM
1.250	0.554	0.557	0.006	0.083
1.000	0.565	0.569	0.011	0.096
0.500	0.613	0.633	0.052	0.137
0.200	0.741	0.812	0.275	0.224
0.125	0.836	0.915	0.479	0.313

Table XVII: DWD and FWHM for the BAC model for several values of applied voltage, as shown in Fig. 25.

V_c (volts)	Y_{min}	Y_{peak}	DWD	FWHM
500	0.258	0.557	0.404	0.181
750	0.577	0.720	0.337	0.203
1000	0.741	0.812	0.275	0.224
1200	0.805	0.847	0.217	0.230

Table XVIII: DWD and FWHM for the BAC model for several values of ion current , as shown in Fig. 26.

I_i (mA)	Y_{min}	Y_{peak}	DWD	FWHM
2.0	0.816	0.853	0.203	0.230
2.8	0.741	0.812	0.275	0.224
5.0	0.501	0.675	0.349	0.195
7.2	0.303	0.572	0.386	0.181

IV. CONCLUSIONS

Langmuir and Blodgett solved poisson's equation for concentric spherical electrodes and discovered the formation of a single virtual electrode at the center electrode [16]. Hirsch performed similar analysis on an IEC device, but included the emission of electrons from the inner surface of the vacuum chamber in his theoretical model. Hirsch's experiments and analysis indicated that a multiple potential well structure existed at the center of the IEC device [11]. Dolan [15],[19], Swanson [13]-[14], and Lavrent'yev [18] developed more realistic models that accounted for spreads in total particle energy and angular particle energy. Following the work of Dolan and Swanson, we have performed computer simulations for the three systems noted in Table IV. We have obtained solutions in a consistent framework, and performed an extensive parametric study of the solutions over $\sigma_{e,\phi}$, $\sigma_{e,E}$, $\sigma_{i,\phi}$, $\sigma_{i,E}$, I_e, I_i, V_a, V_c and the factor β.

Information obtained, from solutions to the models in Table IV, provides insights in IEC performance with respect to which parameters and conditions will be most conducive to double well formation. The results have shown that double well formation requires that $\sigma_{i,\phi}$ for BCA systems and $\sigma_{e,\phi}$ for BAC systems, is relatively small. However, it is not necessarily desirable for $\sigma_{e,\phi}$ or $\sigma_{i,\phi}$ to be small. In that case, the depth of the potential well, $1 - Y_{\min}$, is increased, but the DWD, Eq. (44), is decreased. It could also be noted that double well existence depends weakly on $\sigma_{i,E}$ for BCA systems

and $\sigma_{e,E}$ for BAC systems. In addition, $\sigma_{e,E}$ for BCA systems and $\sigma_{i,E}$ for BAC systems, have very little influence on potential well structure.

In this paper we have concentrated on models that permit extensive parametric studies with respect to double well formations. The models can certainly be improved both in terms of underlying physical phenomena and numerical techniques of solution. Such improvements will permit comparisons with experimental data and more realistic assessments. Nevertheless, the present work clarifies the past work on the problem and provides many useful insights.

REFERENCES

[1]   L. Chacon and G. H. Miley, "Inertial Electrostatic Confinement [3]He Breeder For D-[3]He Satellite Systems," *Fusion Technology*, vol. 33, pp. 182, Mar. 1998.

[2]   B. Bromley, "Approximate Modeling Of The Inertial Electrostatic Confinement Cylindrical Device," M.S. Thesis, University of Illinois Urbana-Champaign, 1997.

[3]   J. B. Javedani, Y. B. Gu, M. J. Williams, J. Hartwell, R. L. Anderl, G. H. Miley, J. H. Nadler, J. L. Jones, R. A. Nebel, and D. C. Barnes, "Studies of the IEC Accelerator-Plasma Target Fusion Neutron Source for Activation Analysis," *Bulletin of the American Physical Society*, vol. 39, no. 7, pp. 1768, 1994.

[4]   G. H. Miley, H. Momota,"A Collimator-Converter System for IEC Propulsion," *Space Technology and Applications International Forum-STAIF 2002*, 2002 , pp. 768-779.

[5]   G. H. Miley, R. Burton, H. Momota, N. Richardson, M. Coventry, Y. Shaban, "High Performance Manned Interplanetary Space Vehicle Using D-[3]He Inertial Electrostatic Fusion", *Space Technology and Applications International Forum-STAIF 2002*, 2002, pp. 819-827.

[6]   R. W. Bussard, "An Advanced Fusion Energy System For Outer-Planet Space Propulsion", *Space Technology and Applications International Forum-STAIF 2002*, 2002, pp. 768-779.

[7]   J. W. Weidner, "The Production of ^{13}N from Inertial Electrostatic Confinement Fusion", M.S. Thesis, University of Wisconsin-Madison, 2003.

[8]   J. W. Weidner, G. L. Kulcinski, J. F. Santarius, R. P. Ashley, G. Piefer, B. Cipiti, R. Radel, S. Krupakar Murali, "Production of 13N via Inertial Electrostatic Confinement Fusion", *Fusion Science and Technology*, vol. 44, pp. 539, 2003.

[9]   G. H. Miley, H. Momota, Y. Shaban, and H. Hora, "Progress in Development of a Converging Beam Neutron Source For Driving a Sub-Critical Fission Reactor", *Proceedings 10th International Conference on Nuclear Engineering*, Arlington, VA, April 14-18, 2002.

[10]   B. Jurczyk, "Theory and Development of a Sealed Deuterium-Tritium Inertial Electrostatic Confinement Neutron Generator," M.S. Thesis, University of Illinois Urbana-Champaign, 1997.

[11] R. L. Hirsch, "Inertial Electrostatic Confinement of Ionized Fusion Gases", *J. of Appl. Phys.*, vol. 38, pp. 4522, Oct. 1967.

[12] D. A. Swanson, B. E. Cherrington, J. T. Verdeyen, "Multiple potential-well structure created by electron injection in spherical geometry," *Appl. Phys. Lett.*, vol. 23, pp. 125, Aug. 1973.

[13] D. A. Swanson, "Theoretical Study of a Spherical Inertial Electrostatic Plasma Confinement Device," Ph. D. Dissertation, University of Illinois-Urbana-Champaign, 1975.

[14] D. A. Swanson, B. E. Cherrington, and J. T. Verdeyn, "Recent Developments In Electrostatic Confinement-Theoretical," *Annals New York Academy of Sciences*, pp. 139, 1973.

[15] T. J. Dolan, "Electrostatic-Inertial Plasma Confinement," Ph. D. Dissertation, University of Illinios-Urbana-Champaign, 1975.

[16] I. Langmuir and K. E. Blodgett "Currents Limited by Space Charge Between Concentric Spheres," *Phys. Rev.*, vol. 24, pp. 49, 1924.

[17] I. Langmuir, and K. T. Compton, "Electrical Discharges in Gases, Part II: Fundamental Phenomena in Electrical Discharges," *Rev. of Mod. Phys.*, vol. 3, no. 2, pp. 246, April 1931.

[18] T. J. Dolan, J. T. Verdeyen, D. J. Meeker, and B. E. Cherrington, "Electrostatic-Inertial Plasma Confinement," *J. Appl. Phys.*, vol. 43, no. 4, pp. 1590, April 1972.

[19] O. A. Lavrent'yev, "Investigation of an Electromagnetic Trap," AEC-tr-7002, (1970).

[20] R. W. Hockney, "Formation and Stability of Virtual Electrodes in a Cylinder," *J. Appl. Phys.*, vol. 39, no. 9, pp. 4166, Aug. 1968.

[21] M. Ohnishi, K. H. Sato, "Correlation Between Potential Well Structure and Neutron Production in Inertial Electrostatic Confinement Fusion," *Nuclear Fusion*, vol. 37, no. 5, pp. 611, 1997.

[22] H. Matsuura, T. Takaki, Y. Nakao, and K. Kudo, "Radial Profile of Neutron Production Rate In Spherical Inertial Electrostatic Confinement Plasmas," *Fusion Technology*, vol. 39, pp. 1167, May 2001.

[23] I.V. Tzonev, "Effect of Large Ion Angular Momentum Spread and High Current on Inertial Electrostatic Confinement Potential Structures," M. S. Thesis, University of Illinois-Urbana-Champaign, 1996.